Mechanism and Machine Theory 81 (2014) 140–154

Contents lists available at ScienceDirect

Mechanism and Machine Theory

journal homepage: www.elsevier.com/locate/mechmt

Design and strength analysis methods of the trochoidal gear reducers

Shuting Li *

Department of Mechanical, Electrical and Electronic Engineering, Interdisciplinary Faculty of Science and Engineering, Shimane University, Matsue 690-8504, Japan

ARTICLE INFO

Article history:
Received 14 January 2014
Received in revised form 5 July 2014
Accepted 7 July 2014
Available online 26 July 2014

Keywords:
Cycloid gear
Trochoidal gear
Design
Contact analysis
Strength calculations

ABSTRACT

This paper deals with design and strength analyses of trochoidal gear reducers. At first, design software is developed to conduct geometric design of the trochoidal gear reducers in AutoCAD software surrounding. With the help of developed software, gearing parameters and structural dimensions of the trochoidal gear reducers can be determined very simply. Two-dimensional (2D), drawings of the designed reducers can be drawn by the software automatically. Three-dimensional (3D), drawings of the designed reducers can also be drawn very quickly with 3D commands of AutoCAD software when the 2D drawings are available. The developed software can not only save much time of designers, but also makes it possible for inexperienced designers to be able to design the trochoidal gear reducers freely. Secondly a new mechanics model and finite element method (FEM) are presented in this paper to conduct loaded gear contact analysis of the trochoidal gear reducers in order to solve strength calculation and evaluation problems of the reducers. With the help of the model and FEM presented, it becomes practical to be able to conduct loaded gear contact analysis and strength calculations of the trochoidal gear reducers in theory. FEM software is developed based on the model and method. With the help of the developed FEM software, loads and contact stresses distributed on teeth, bushes and rollers of the trochoidal gear reducers are analyzed successfully. Bending stresses of the trochoidal gear are also analyzed, though it is rare for the reducer to have bending failures.

1. Introduction

Trochoidal gear reducers, usually called cycloid gear speed reducers, have found wide applications in industry robots and other aspects because of the advantages of small backlash, high transmission accuracy, large reduction ratio, high torsional rigidity, great load capacity and high shock-resistant ability. Though it has passed more than 70 years since its invention of the reducer by Mr. *Lorenz Braren* and many units of this reducer have been made and used now, many design problems of this reducer have not been solved so far. Specially, strength calculation methods of this reducer have not been found so far in theory.

Lehman [1] conducted theoretical analysis of tooth load distribution of a cycloid speed reducer. Though tooth load distribution was obtained by Lehman, his method cannot be used in real design of a cycloid speed reducer because structural deformation of the cycloid gear was not considered in his research. Also, loads distributed on bushes and center bearing rollers of the cycloid speed reducer could not be studied by Lehman. Malhotra and Parameswaran [2] also conducted a theoretical study on load analysis and efficiency calculation of a cycloid speed reducer roughly using an analytical method. Like Lehman's research, since the effect of the structural deformation of the cycloid gear could not be considered in their analyses, an accurate distribution of loads on teeth could not be obtained. Of course, the effect of the machining tolerances and tooth profile modification of the cycloid speed reducer on tooth load distribution could not be

* Tel./fax: +81 0852 328908.
E-mail address: shutingli@ecs.shimane-u.ac.jp.

http://dx.doi.org/10.1016/j.mechmachtheory.2014.07.001
0094-114X/

studied. Yang and Blanche [3,4] studied the effect of machining tolerances on backlash distribution of the cycloid speed reducers. Ishida et al. [5] firstly made a try to use commercial software of the FEM to analyze tooth loads of a new type of cycloid gear speed reducer (usually called RV speed reducer [6]). Since a very long time was needed to complete the analysis using the commercial software and it is very difficult to find correct contact states of the teeth and rollers, Li [7,8] developed a special FEM for tooth load analysis of the RV speed reducer based on a very long experience on FEM programming. With the help of the developed FEM software, tooth loads of the RV speed reducer were analyzed very simply and quickly. It also became possible to investigate effects of tooth width, gear size, machining tolerances and loading torque on tooth load distribution of the RV speed reducer [9,10].

Though the above-mentioned studies can be found, the real loads distributed on teeth, bushes and center bearing rollers of a trochoidal gear reducer cannot be analyzed. Of course, it is still an unsolved problem how to conduct strength calculations and evaluation of the trochoidal gear reducer when designing it.

This paper presents a new model and a new FEM to conduct loaded gear contact analysis of the trochoidal gear reducers. Based on the model and method presented, special FEM programs have been developed. With the help of the developed FEM programs, loaded gear contact analyses are conducted and loads distributed on teeth, bushes and center bearing rollers are obtained. Contact stresses on the teeth, bushes and rollers are calculated with the *Hertzian*'s formula and bending stresses of the trochoidal gear are analyzed with FEM when the loads on the teeth, bushes and rollers are known.

2. Typical structure concept of a trochoidal gear reducer

Fig. 1 is a typical structure concept of a trochoidal gear reducer used as an example in this paper. This reducer consists of one external spur gear, 34 pins (also called pin gear), 5 bushes, 5 carrier shafts, 13 rollers and one crankshaft. Since the external spur gear uses the trochoidal curve as the tooth profile, here it is simply called the trochoidal gear. On the trochoidal gear, there are 5 holes used to insert the 5 bushes so, these holes are called bush holes in this paper.

In Fig. 1, the pin gear is used as an internal spur gear to engage with the trochoidal gear. Usually the number of pins is one greater than the number of teeth of the trochoidal gear. The 5 bushes are mounted on the 5 carrier shafts. The bushes are used as the sliding bearings between the carrier shafts and the bush holes. The crankshaft is inserted into the center hole on the trochoidal gear. It is used to produce eccentric movement of the trochoidal gear. The 13 rollers are inserted between the center hole and the crankshaft. They are used as rolling bearing without the inner and the outer rings.

Eccentric direction of crankshaft is defined as an angle between the Y-axis (vertical axis) and the eccentric direction of the crankshaft (the angle θ as shown in Fig. 7). This angle is called *crankshaft angle* in this paper. For the case as shown in Fig. 1, eccentric direction of crankshaft is along the Y-axis. At this case, the crankshaft angle is 0°.

3. Geometric design of trochoidal gear reducers

Based on the principle of kinematics of the trochoidal gear reducer, software used for geometrical design and dimension calculations of the trochoidal gear reducer has been developed successfully in AutoCAD surrounding using the Visual Basic language inserted in AutoCAD software. With the help of the developed software, trochoidal gear reducers can be designed and calculated very simply and quickly. After the design procedure is finished, the designed gear parts or the reducer structure can be drawn automatically on the template of the AutoCAD software.

Figs. 2, 3 and 4 are examples of 2D and 3D drawings of the gears and the reducers designed by the developed software. Fig. 2(a) is a 2D drawing of the designed trochoidal gear. Fig. 2(b) is a 3D drawing of the design trochoidal gear. This 3D drawing is made using 3D commands in the AutoCAD software based on the 2D drawing as shown in Fig. 2(a). Fig. 3(a) and (b) is 2D and 3D drawings of the

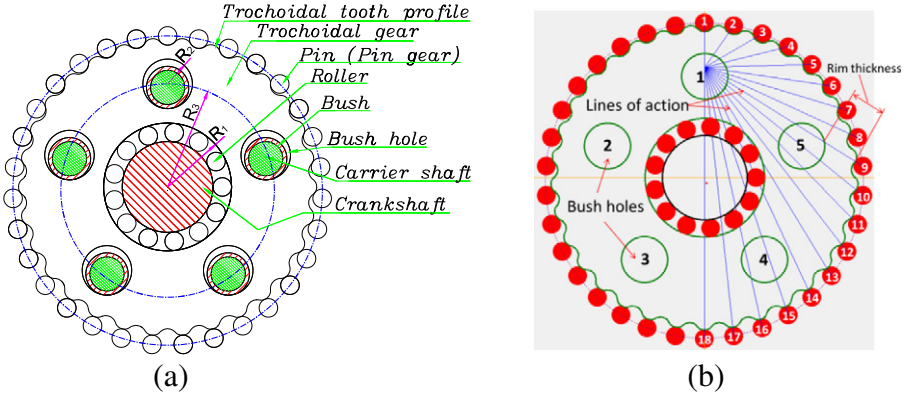

Fig. 1. A typical structure concept of a trochoidal gear reducer.

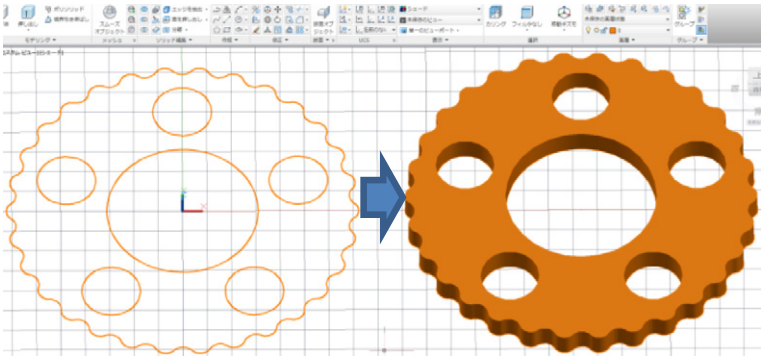

Fig. 2. 2D and 3D drawings of the trochoidal gear.

trochoidal gear engaging with the pin gear respectively. Fig. 4(a) and (b) is 2D and 3D drawings of the reducer respectively. These drawings can be made in a very short time on the template of the AutoCAD software when the design procedure is ended.

4. Loaded gear contact analyses of the reducer

Since strength calculation problems of the trochoidal gear reducers have not been solved so far and it has been still quite a difficult problem to find a suitable method to do 3D strength analyses of the trochoidal gear reducers in theory, this paper presents a 2D FEM to do loaded gear contact analyses and strength calculations of the trochoidal gear reducers approximately. This is because the reducer can be regarded as a 2D problem approximately.

Loads distributed on the teeth, bushes and rollers can be obtained through the loaded gear contact analyses of the reducer. Then contact stresses on the teeth, bushes and rollers can be calculated using *Hertzian*'s formula of elastic contact theory and bending stresses of the trochoidal gear can also be analyzed using the FEM. The main procedures of the loaded gear contact analyses of the trochoidal gear reducers are stated in the following.

4.1. Mechanics model used for loaded gear contact analysis

Mechanics model used for loaded gear contact analysis of the trochoidal gear reducer is presented as shown in Fig. 5 based on the principle of kinematics of the trochoidal gear reducer. In Fig. 5, contact rigidity between the pins and the teeth of the trochoidal gear can be replaced by many springs attached on surfaces of the teeth of the trochoidal gear. Stiffness coefficients of these springs are denoted by K_{pin} and it is assumed approximately that all the springs on the teeth have the same stiffness coefficients K_{pin} [11]. These springs are attached at the contact points between the pins and the teeth and along the lines of action of themselves as shown in Fig. 5. The number of springs is equal to the number of the contact teeth in theory. In the same way, contact rigidity between the bushes and the bush holes can be replaced by 5 springs. Stiffness coefficients of these springs are denoted by K_{bush}. These springs are attached at the contact points between the bushes and the bush holes along the directions of the normal lines of the contact points. The number of springs K_{bush} is equal to the number of the bush holes. The contact rigidity among the center hole of the trochoidal gear,

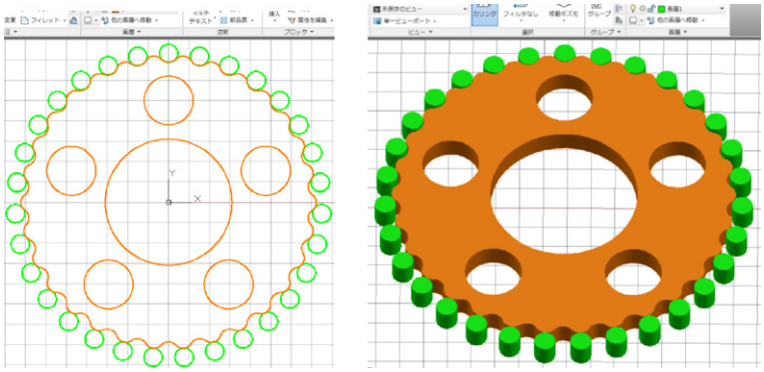

Fig. 3. 2D and 3D of drawings of the trochoidal gear engaging with pin gear.

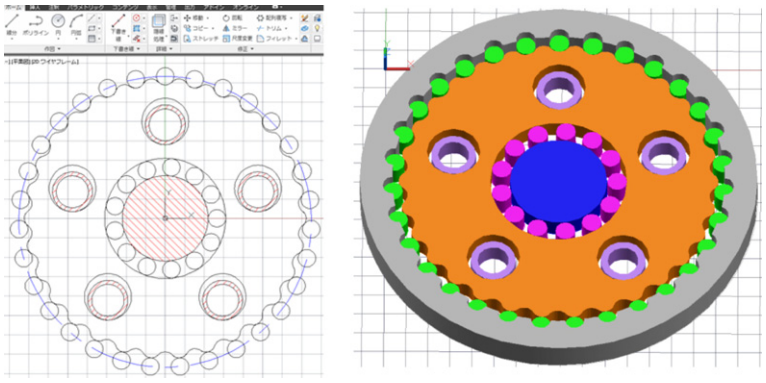

(a) 2D drawing (b) 3D drawing

Fig. 4. 2D and 3D drawings of the trochoidal gear reducer.

the rollers and the crankshaft can also be replaced by many springs with the stiffness coefficients denoted by K_{roller} as shown in Fig. 5. These springs are attached at the contact points between the center hole and rollers along the directions of the normal lines of the contact points.

K_{pin}, K_{bush} and K_{roller} can be calculated approximately using elastic contact theory of *Hertzian*. Though the contact rigidity between two elastic bodies is non-linearity of the normal load, it can be treated as a linear stiffness spring approximately when the normal load is not so great and this treatment has enough accuracy for an engineering calculation [11]. So, K_{pin}, K_{bush} and K_{roller} are constants used in this paper.

In order to be able to consider the effects of machining tolerances and tooth profile modification of the trochoidal gear, clearances are added at the free ends of the springs K_{pin} as shown in Fig. 5. Since different clearances can be given to the different springs K_{pin}. With the help of these clearances, it can be realized simply to consider the effects of the machining tolerances and tooth profile modification of the trochoidal gear in loaded gear contact analyses of the reducer.

4.2. Relationship between tooth loads and transmitted torque

Fig. 6 is used to explain the relationship between tooth loads and transmitted torque *T*. In Fig. 6, the pitch point of the trochoidal gear is denoted by *P* and the lines of action of the contact teeth are also illustrated. According to the principle of kinematics of the trochoidal gear, all the lines of action can be drawn from the centers of the pins to the pitch point *P* as shown in Fig. 6. So, all the lines of action can be positioned geometrically.

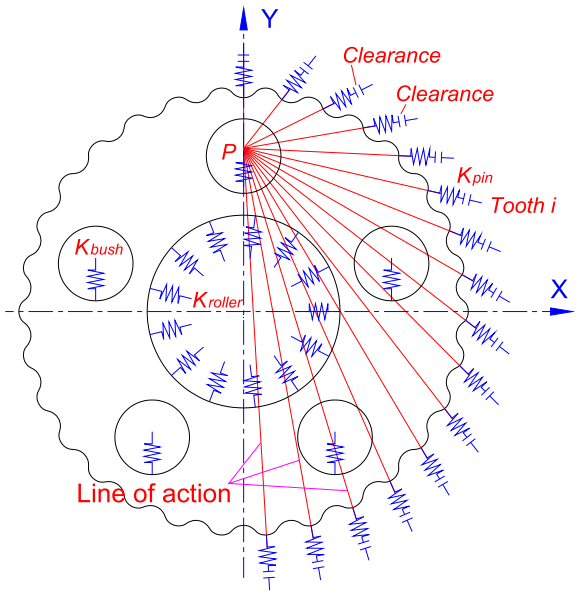

Fig. 5. Mechanics model used for loaded gear contact analysis.

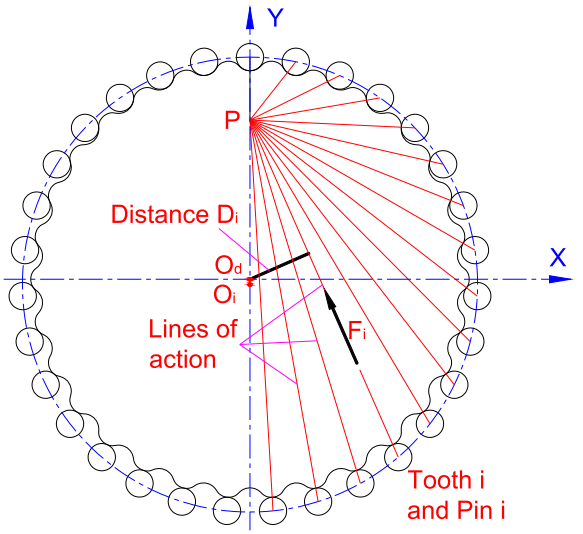

Fig. 6. Relationship among the pitch point, the line of actions and tooth loads.

In Fig. 6, the rotational center of the trochoidal gear is denoted by O_d and the rotational center of the pin gear is denoted by O_i. O_dO_i is the eccentricity. If the distance from the point O_d to the line of action of the tooth i is denoted by D_i and tooth load on the tooth i is denoted by F_i as shown in Fig. 6, transmitted torque T can be calculated with the following Eq. (1).

$$T = \sum_{i=1}^{n}(F_i \times D_i) \qquad \left(i = 1,2,3,\ldots,n; n = \frac{Z_2}{2} + 1\right) \tag{1}$$

In Eq. (1), Z_2 is the number of pins. Eq. (1) is the equilibrium relationship between transmitted torque T and tooth loads. Since the tooth load F_i can be expressed using the Eq. (2), then the torque T can be calculated with Eq. (3) by substituting Eq. (2) into Eq. (1).

$$F_i = \Delta d_i \times K_{pin} (i = 1,2,3,\ldots,\ n) \tag{2}$$

$$T = \sum_{i=1}^{n}\left(\Delta d_i \times K_{pin} \times D_i\right) \qquad (i = 1,2,3,\ldots,n) \tag{3}$$

In Eq. (2), Δd_i is deformation of the spring K_{pin} along the line of action of the tooth i. Δd_i can be available through calculating the relative displacement of the two ends of the spring K_{pin} of the tooth i along the line of action. Displacements of the two ends of the spring K_{pin} of the tooth i along the line of action can be obtained by the finite element analysis when the loads on the teeth, bush holes and center hole of the trochoidal gear are known through loaded gear contact analysis.

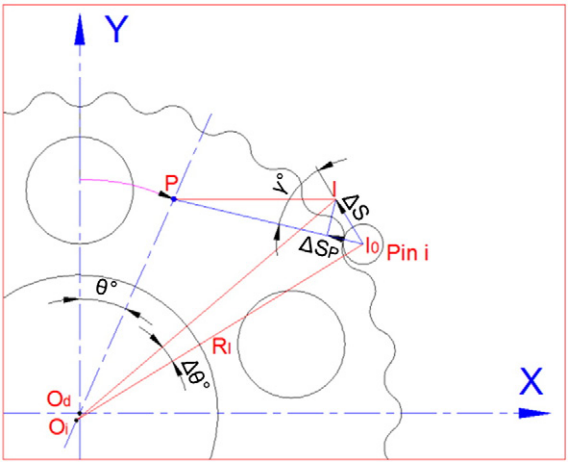

Fig. 7. Displacement of the pin center I_o.

Contact loads on the bushes and rollers are reaction loads resulted from the tooth loads as shown in Fig. 5 in order to keep a load balance with the tooth loads. These reaction loads can be calculated in the same way as the tooth loads when displacements of two ends of the springs K_{bush} and K_{roller} are known.

4.3. Tooth contact deformation

Fig. 7 is used to explain tooth contact deformation of the reducer. According to the elastic contact theory of *Hertzian*, it can be assumed that the pins have only local deformation between the contact surfaces. So, all the pin centers can be considered to be on a rigid circle. If this rigid circle has an angular deformation denoted by $\Delta\theta$ under the transmitted torque T, then all the pin centers shall have the same circumferential displacement ΔS and ΔS can be calculated using Eq. (4). Here, R_I is the radius of the rigid circle (= radius of the circle of the pin centers).

$$\Delta S = \Delta\theta \times R_I \tag{4}$$

As shown in Fig. 7, if the crankshaft is rotated in a clockwise direction from the Y-axis to an angle θ, the eccentric direction of the crankshaft is changed from the Y-axis to the direction of the angle θ. Then the pitch point P of the trochiodal gear shall also be changed from the Y-axis to a new position denoted by P in Fig. 7. If the center of pin i is denoted by I_0 as shown in Fig. 7, then the line PI_0 is the new position of the line of action of the pin i. At this time, if the angle between the line PI_0 and the tangential line of the pin center circle are denoted by γ and the displacement component of pin center I_0 along the line PI_0 is denoted by ΔS_P, then the following Eq. (5) can be obtained.

Eq. (5) means that if ΔS and γ are known, the displacement component of all the pin centers relative to the trochoidal gear along the lines of action of themselves can be calculated.

$$\Delta S_P = \Delta S \times \cos\gamma \tag{5}$$

4.4. FEM modeling

In order to make the FEM programs used for loaded gear contact analysis simpler, the springs on the teeth, bush holes and center hole as shown in Fig. 5 are replaced by a lot of special two-triangle elements. With these two triangle elements, the mechanics model of the reducer as shown in Fig. 5 can be changed into FEM model as shown in Fig. 8. These two-triangle elements are called boundary contact elements (BCE). The nodes on the free ends of the BCE are called boundary nodes as illustrated in Fig. 8. The BCE have a special meaning in this paper. Like the springs, the BCE on the teeth are attached along the lines of action and the BCE on the bush holes and the center hole are attached along the normal lines of the contact points. It has been confirmed that this treatment provides a great convenience to the FEM programming and leads to a success of the loaded gear contact analysis of the trochoidal gear reducer.

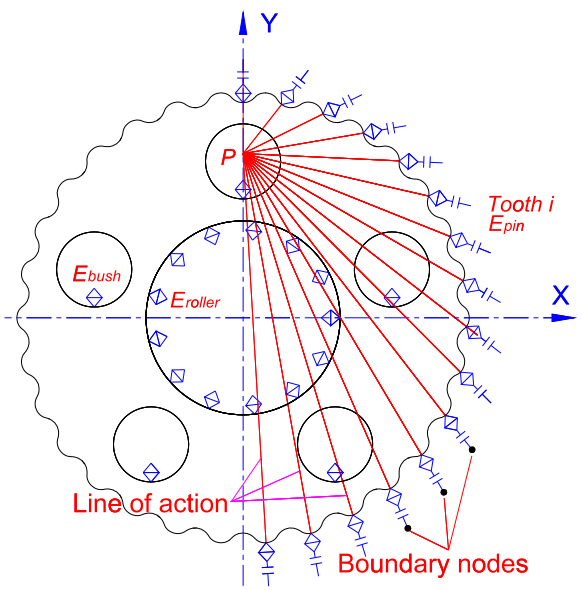

Fig. 8. FEM model used for loaded gear contact analysis.

In order to let the BCE have the same elasticity as the springs, the Young's modules of the BCE are determined according to the stiffness coefficients of K_{pin}, K_{bush} and K_{roller} respectively and have nothing to do with the materials used. This means that the Young's modules of the BCE are different from that of the trochoidal gear body. Of course, the Young's module of the gear body is determined according to the gear material used. In the paper, the Young's module of the trochoidal gear body is 196GPa. The Young's modules of the BCE on the teeth, bush holes and center are denoted by E_{pin}, E_{bush} and E_{roller} respectively in Fig. 8.

2D, triangle element is used to divide FEM meshes of the gear body as shown in Fig. 9 since the BCE also used the same element. Fig. 9 is one of the mesh-dividing patterns used for FEM analysis. As shown in Fig. 9, all the teeth and holes are well mesh-divided with the help of the triangle element. Special software is developed to do this mesh-dividing automatically. Of course, a very long time was spent to finish the development of the mesh-dividing software. With the help of this software, FEM model and mesh-dividing can be made automatically at any eccentric position of the gear when the gearing parameters and structural dimensions are given.

In Fig. 9, BCE on the teeth, bush holes and center hole are numbered. These numbers are used to illustrate positions of the teeth, bushes and rollers in calculation results stated later.

4.5. Static equilibrium equations of the FEM

Static equilibrium equations of the FEM model in Fig. 9 can be expressed as Eq. (6) according to the principle of the FEM. In Eq. (6), $\{R_i\} = \{R_1, R_2, R_3, \ldots, R_n\}^T$ is an array of nodal loads of the FEM. $\{\delta_i\} = \{\delta_1, \delta_2, \delta_3, \ldots, \delta_n\}^T$ is an array of nodal displacements of the FEM. K_{ij} ($i = 1, 2, \ldots, n$; $j = 1, 2, \ldots, n$) is coefficient of stiffness matrix $[K_{ij}]$ of the FEM. For a two-dimensional FEM problem, δ_i and R_i can be expressed as $\delta_i = [U_i\ V_i]^T$, $R_i = [R_{ix}\ R_{iy}]^T$. U_i and V_i are deformation components of the node i in the directions of X-axis and Y-axis respectively. R_{ix} and R_{iy} are the load components of node i in the directions of X-axis and Y-axis respectively.

Eq. (6) cannot be solved if the boundary conditions are not given. So, the following important step is how to give the boundary conditions to the boundary nodes in Eq. (6). This is stated in the following section.

$$\begin{bmatrix} K_{11} & K_{12} & \cdots & K_{1i} & \cdots & K_{1n} \\ K_{21} & K_{22} & \cdots & K_{2i} & \cdots & K_{2n} \\ \vdots & \vdots & \vdots & \vdots & \vdots & \vdots \\ K_{i1} & K_{i2} & \cdots & K_{ii} & \cdots & K_{in} \\ \vdots & \vdots & \vdots & \vdots & \vdots & \vdots \\ K_{n1} & K_{n2} & \cdots & K_{ni} & \cdots & K_{nn} \end{bmatrix} \times \begin{Bmatrix} \delta_1 \\ \delta_2 \\ \vdots \\ \delta_i \\ \vdots \\ \delta_n \end{Bmatrix} = \begin{Bmatrix} R_1 \\ R_2 \\ \vdots \\ R_i \\ \vdots \\ R_n \end{Bmatrix} \tag{6}$$

4.6. Boundary conditions of FEM analysis

In order to give the boundary conditions to the boundary nodes of BCE attached on the surfaces of the teeth, bush holes and center hole along the normal lines of the contact points (directions of the lines of action for the boundary nodes of BCE on

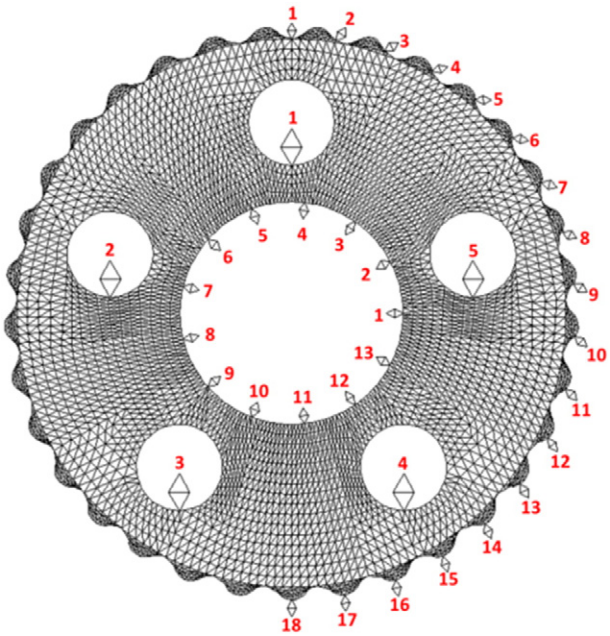

Fig. 9. FEM Mesh-diving pattern (Elements = 8718 Notes = 5097).

tooth surface and radial directions for the boundary nodes of BCE on the surfaces of the bush holes and center hole), many local coordinate systems are built up in the global coordinate system (O-XY) for the boundary nodes individually. For example, for the boundary node *I* of BCE attached on the center hole surface as shown in Fig. 10 (node *I* can be regarded as the contact point between roller *I* and the crankshaft surface), the local coordinate system (O-X*Y*) is built in this way. The Y* axis passes through the origin O of the global coordinate system (O-XY) and is along the radial direction of the node *I*. The X* axis passes through the origin O and is vertical to the Y* axis. This means that the local and the global coordinate systems have the same origin at the gear center O. The angle between X axis and X* axis is denoted by α. In the local coordinate system (O-X*Y*), if the displacements of node *I* in the directions of X* axis and Y* axis are denoted by $\delta_i^* = [U_i^* \; V_i^*]^T$ respectively, the boundary conditions of node *I* can be given in the following way.

Since node *I* can only carry radial compressive load and is free in tangential direction at the contact point on the surface of the crankshaft, these boundary conditions cannot be given simply in the global coordinate system (O-XY), but they can be given simply in the local coordinate system (O-X*Y*) through letting $V_I^* = 0$ and U_I^* be free. Boundary conditions of other boundary nodes can also be given in the same way through building their local coordinate systems (O-X*Y*). Since many different local coordinate systems are built up in the global coordinate system in order to give the boundary conditions of the boundary nodes, it is necessary to connect these local coordinate systems with the global coordinate system when the FEM analysis is conducted. This connection is realized through coordinate transformation method stated in the following.

In the local coordinate system (O-X*Y*) as shown in Fig. 10, the load on the node *I* in the directions of X* axis and Y* axis can be denoted by $R_i^* = [R_{ix}^* \; R_{iy}^*]^T$. According to the principle of coordinate transformation, nodal displacements $\delta_i = [U_i \; V_i]^T$ of node *I* in the global coordinate system can be calculated by Eq. (8) using the nodal displacements δ_i^* in the local coordinate system where, *L* is called coordinate transformation matrix. It can be expressed as Eq. (9). In Eq. (9), α is the angle between the X axis and X* axis. In the same way, nodal loads $R_i = [R_{ix} \; R_{iy}]^T$ of node *I* in the global coordinate system can be calculated by Eq. (10) using $R_i^* = [R_{ix}^* \; R_{iy}^*]^T$ of node *I* in the local coordinate system.

$$\delta_i = L \times \delta_i^* \tag{8}$$

$$L = \begin{bmatrix} \cos\alpha & -\sin\alpha \\ \sin\alpha & \cos\alpha \end{bmatrix} \tag{9}$$

$$R_i = L \times R_i^* \tag{10}$$

Substituting Eq. (8) and Eq. (10) into Eq. (6), Eq. (11) can be obtained. Eq. (11) is a special static equilibrium equation in that the local coordinate system (O-X*Y*) and the global coordinate system (O-XY) exist at the same equation. With the help of this special equation, boundary conditions of the boundary node *I* can be given simply in the local coordinate system directly. Boundary conditions of the other boundary nodes can also be given in the same way as node *I*. After all the boundary conditions of the boundary

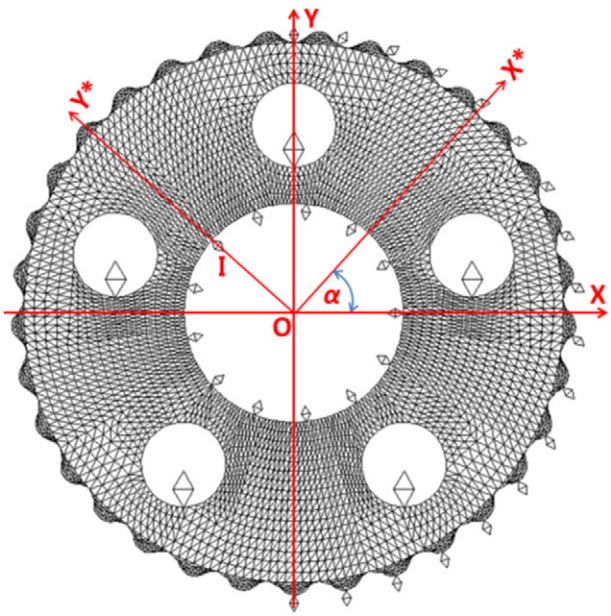

Fig. 10. Relationship between the local coordinate system and the global coordinate system.

nodes are given, a special static equilibrium equation with many local coordinate systems in the global coordinate system like the Eq. (11) can be available. When this special equation is solved as usual, deformation of all the nodes can be available. Then tooth loads can be calculated with Eq. (2) when the deformation of all the boundary nodes is known. Loads on the bushes and rollers can also be calculated in the same way as the tooth loads. A flowchart of the FEM programming used for loaded gear contact analysis is introduced in detail in the following.

$$\begin{bmatrix} K_{11} & K_{12} & \cdots & K_{1i}L & \cdots & K_{1n} \\ K_{21} & K_{22} & \cdots & K_{2i}L & \cdots & K_{2n} \\ \vdots & \vdots & \vdots & \vdots & \vdots & \vdots \\ L^T K_{i1} & L^T K_{i2} & \cdots & L^T K_{ii} L & \cdots & L^T K_{in} \\ \vdots & \vdots & \vdots & \vdots & \vdots & \vdots \\ K_{n1} & K_{n2} & \cdots & K_{ni}L & \cdots & K_{nn} \end{bmatrix} \times \begin{Bmatrix} \delta_1 \\ \delta_2 \\ \vdots \\ \delta_i^* \\ \vdots \\ \delta_n \end{Bmatrix} = \begin{Bmatrix} R_1 \\ R_2 \\ \vdots \\ R_i^* \\ \vdots \\ R_n \end{Bmatrix} \tag{11}$$

4.7. Procedures of the loaded gear contact analysis

Procedures of the loaded gear contact analysis of the trochoidal gear reducer are as follows.

Step 1: All the boundary nodes of the BCE in the parts of bush holes and center hole are fixed firstly only in the directions of the normal lines of themselves at the contact points and free in the vertical directions of the normal lines in the local coordinate systems.

Step 2: An optional angular deformation $\Delta\theta$ is given. ΔS is calculated by Eq. (4) and ΔS_p is calculated by Eq. (5) for every boundary node of the BCE on the tooth surface. ΔS_p is given as displacement boundary conditions to the boundary nodes of the BCE on the tooth surface along the lines of action of themselves in the local coordinate systems. If it is necessary to consider the machining tolerances and tooth profile modification of the trochoidal gear in the FEM analysis, the machining tolerances and quantity of the tooth profile modification are given as the displacement boundary conditions to the boundary nodes of the BCE on the tooth surface like ΔS_p at the same time.

Step 3: The special static equilibrium equation like Eq. (11) is formed and solved when all the boundary conditions are given. Then reaction loads on the boundary nodes of the BCE attached on the bush holes and center hole are available after the special static equilibrium equation is solved. Deformation of the boundary nodes of the BCE on the tooth surface along the lines of action can be available also.

Step 4: If the reaction loads on the boundary nodes of the BCE attached on the surfaces of the bush holes and the center hole are tensile, this means that these boundary nodes should be free in the next one calculation since these boundary nodes cannot carry the tensile loads otherwise these points should be fixed continually in the next one calculation. A similar judgment is also made for all the boundary nodes of the BCE on tooth surface. For the boundary nodes on the teeth, if deformation of a boundary node along the line of action is toward the pitch point P and this deformation is greater than the sum of the ΔS_p and the clearance resulted from the machining tolerances and tooth profile modification, it means that this tooth is contacting with the pin and the tooth load can be calculated with Eq. (2) otherwise this tooth is not contacting with the pin and the load on this tooth is zero. The same judgment is made for all the pairs of the contact teeth (the teeth from 1 to 18 as shown in Fig. 9).

Step 5: Transmitted torque of the contact teeth is calculated by Eq. (3).

Step 6: Two important checks are made in this step. The first check is to check current contact states of the pins, bushes and rollers. If the contact states of the pins, bushes and rollers have no more changes by comparing with the contact states obtained in the last one calculation, this means that the FEM analysis can be ended. Otherwise, the current contact states of the pins, bushes and rollers are used as the new boundary conditions given to the boundary nodes of BCE attached on the surfaces of the teeth, bush holes and the center hole, then procedures from Step 2 to Step 6 are repeated until the contact states of the pins, bushes and rollers have no more changes by comparing with the last one calculation. The second check is to check whether the transmitted torque obtained by Eq. (2) is equal to the expected one. If the transmitted torque is not equal to the expected one, $\Delta\theta$ is changed and the procedures from Step 2 to Step 5 are repeated until the transmitted torque is equal to the expected one. If the above two checks are satisfied, then end the analyses and go to Step 7.

Step 7: Output loads on the teeth, bushes and rollers and calculate contact stresses on the teeth, bushes and rollers with *Hertzian*'s formula.

5. Strength calculations of the trochoidal gear reducer

5.1. Gearing parameters and structural dimensions of the reducer used as research objects

Gearing parameters and structural dimensions of the reducer used as research object are given in Table 1. In Table 1, R_1, R_2 and R_3 are radius of the center hole, radius of the bush holes and radius of the center circle of the bush holes respectively. They are indicated in Fig. 1. Applied torque on the trochoidal gear is 200 nm. Calculation results are stated in the following.

As stated above, machining tolerances and tooth profile modifications of the trochoidal gear can also be considered in the finite element analyses with the methods presented in this paper. But, since it needs a lot of space to state clearly the problems of the effects of the machining tolerances and tooth profile modifications on contact strength of the trochoidal gear reducer, these problems shall be investigated in the next one paper in detail.

Table 1
Gearing parameters and structural dimensions of the trochoidal gear reducer.

Gearing parameters	Trochoidal gear Z_1	Pin gear Z_2
Number of teeth and pins	33	34
Pin center diameter (mm)	–	165
Pin radius R (mm)	–	4
Coefficient of tooth shape X	0.279	–
Eccentricity e (mm)	1.75	–
Number of the bush holes	5	–
Number of the rollers	13	–
Radius of the center hole R_1 (mm)	31	–
Radius of the bush holes R_2 (mm)	12	–
Radius of center circle of bush holes R_3 (mm)	53	–
Face width of the trochoidal gear B (mm)	20	–
Applied torque on the torchoidal gear T (N·m)	200	

5.2. Loads distributed on the teeth, bushes and rollers

FEM software has been developed according to the procedures stated in Section 4.7. With the developed FEM software, loaded gear contact analysis is conducted for the reducer as shown in Table 1 at the engagement position that the eccentric direction of the trochoidal gear is toward the Y-axis as shown in Fig. 1. Of course, the FEM software has been developed to be able to conduct the loaded gear contact analysis of the reducer when the trochoidal gear is engaged with the pins at an arbitrary eccentric direction.

Fig. 9 is the mesh-dividing pattern of the reducer used in the contact analysis. As shown in Fig. 9, 18 pins, 5 bushes and 13 rollers are used in the contact analysis.

Fig. 11 is calculated loads on the contact teeth. In Fig. 11, the abscissa is the number of contact teeth indicated in Fig. 1(b) and Fig. 9. The ordinate is the calculated loads on the contact teeth. From Fig. 11, it is found that the loads on the contact teeth are different. The maximum load happened on tooth No. 12. Fig. 11 also indicates that there is a certain reduction of the load on tooth No. 9. This is because of the existence of bush hole No. 5 as shown in Fig. 1(b). In Fig. 1(b), it is found that bush hole No. 5 is just located at the position below tooth No. 9. Since rim thickness along the line of action of tooth No. 9 is the thinnest among the teeth around bush hole No. 5, contact rigidity of tooth No. 9 with the pin along the line of action is weakest. So, the load on tooth No. 9 is lower than the loads on the teeth No. 8 and 10. It has been found by calculations that the load on tooth No. 9 becomes greater when the radius of bush hole No. 5 becomes larger and also it becomes lower when the radius becomes smaller. This phenomenon shall be reported in the next one paper in detail.

Fig. 12 is calculated loads on the bush holes. In Fig. 12, the abscissa is the number of bush holes indicated in Fig. 9. The ordinate is the calculated loads on bushes. From Fig. 12, it is found that loads on bushes No. 1 and No. 5 are zero. This means that these bushes do not work at this eccentric position. The maximum load happened on bushes No. 3 and No. 4. Also, bush No. 2 carries greater loads.

Fig. 13 is calculated loads on the rollers. In Fig. 13, the abscissa is the number of rollers indicated in Fig. 9. The ordinate is the calculated loads on the rollers. From Fig. 13, it is found that the maximum load happened on the roller No. 1. Loads on the rollers from No. 5 to No. 11 are zero. This means that these rollers do not work at this eccentric position.

5.3. Contact stress and contact strength analyses

When the loads on the teeth, bushes and rollers are available, contact stresses on the teeth, bushes and rollers can be calculated using *Hertzian*'s formula of the elastic contact theory. Then contact strength of the teeth, bushes and rollers can be

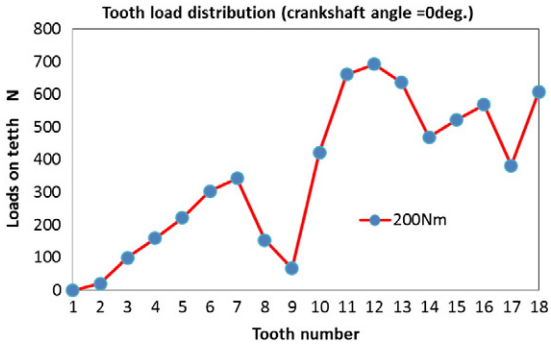

Fig. 11. Tooth load distribution.

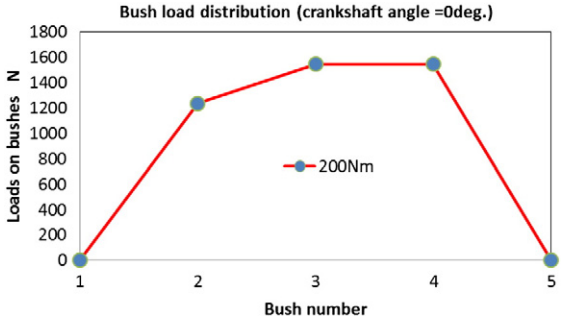

Fig. 12. Bush load distribution.

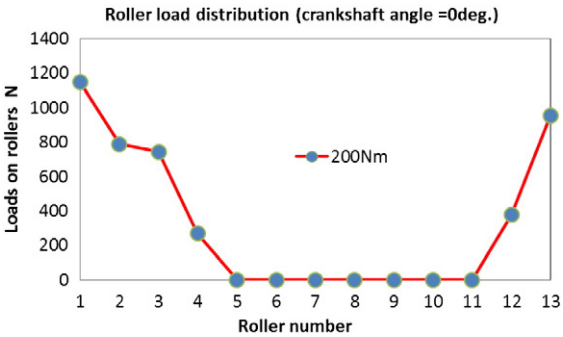

Fig. 13. Roller load distribution.

evaluated by comparing the maximum contact stresses on the teeth, bushes and rollers with the allowable contact stresses of the materials used.

Fig. 14 is calculated contact stresses on the teeth. From Fig. 14, it is found that tooth No. 12 has the maximum contact stress 736 MPa.

Fig. 15 is calculated contact stresses on the bushes. From Fig. 15, it is found that bushes No. 3 and No. 4 have the same maximum contact stress 199 MPa.

Fig. 16 is calculated contact stresses on the rollers. From Fig. 16, it is found that roller No. 1 has the maximum contact stress 745 MPa.

For a trochoidal gear reducer, usually the maximum contact stress on the teeth is much greater than that on the bushes and rollers. So, it is only necessary to evaluate contact strength of the teeth by comparing the maximum contact stress of the teeth with the allowable contact stress of the teeth with the pins. In this paper, it is found that the maximum contact stress on the rollers is a little greater than that on the teeth, so it is also necessary to evaluate the contact strength of the rollers for the reducer used in this paper.

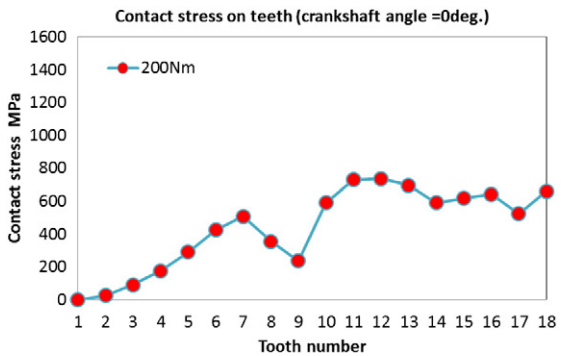

Fig. 14. Tooth contact stress distribution.

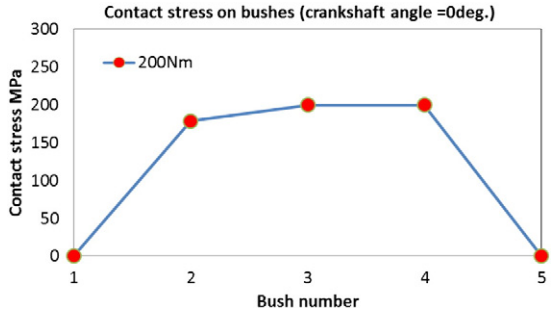

Fig. 15. Bush contact stress distribution.

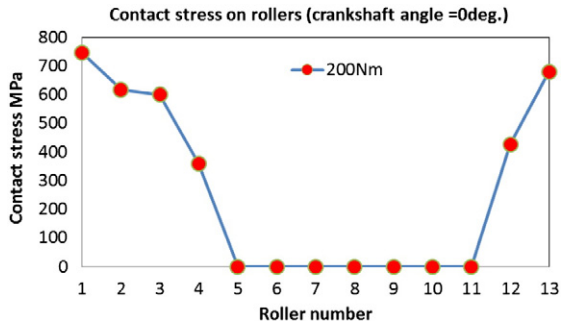

Fig. 16. Roller contact stress distribution.

5.4. Bending stress and strength calculations

When the loads on the teeth, bushes and rollers are known, bending stresses of the trochoidal gear reducer can be analyzed simply by FEM. Figs. 17 and 18 are contour line graphs of the equivalent stress and the maximum principal stress σ_1 distributed on the trochoidal gear. From Fig. 17, it is found that the maximum equivalent stress is located at the contact point between the bush and bush hole No. 5. From Fig. 18, it is found that the maximum value of σ_1 is not located at the contact points of the gear with the pins, bushes and rollers.

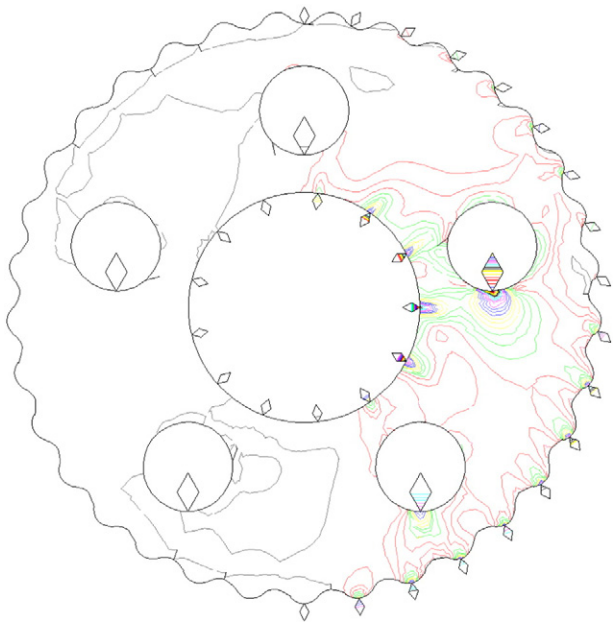

Fig. 17. Contour lines of the equivalent stress of the gear.

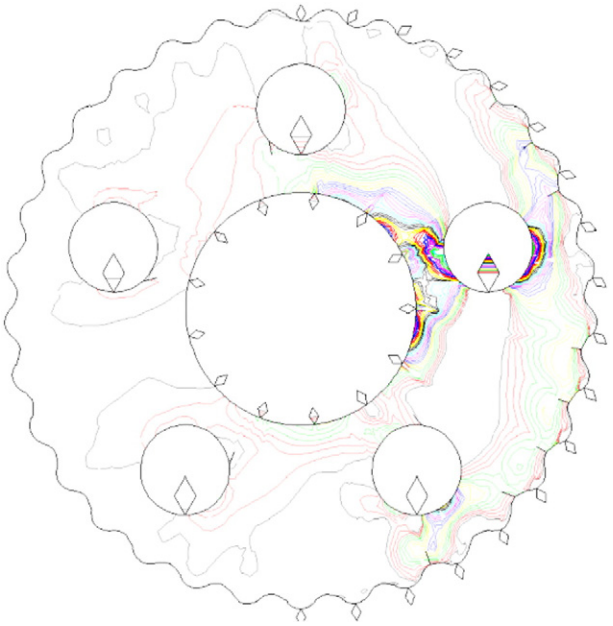

Fig. 18. Contour lines of the maximum principal stress σ_1 of the gear.

Since bending failures of the trochoidal gear almost did not occur in real applications of the trochoidal gear reducers, usually, it is not necessary to evaluate the bending strength of the trochoidal gear in the design procedures. But when the bush holes are made very large and the large holes make the rim or thickness between the bush holes and the center hole very thin, the bending failures may occur. At this time, it is necessary to evaluate the bending strength as well as the contact strength of the reducer in the design procedures.

6. Effects of eccentric direction of the crankshaft on contact stresses

In order to investigate the effects of eccentric direction of the crankshaft on the contact strength of the reducers, loaded gear contact analyses are also conducted for the reducer when the crankshaft angles are 15 and 44°. Calculation results are given in the following.

Figs. 19(a) and (b) are graphs of the tooth engagements of the reducer when the crankshaft angles are 15 and 44° respectively.

Figs. 20(a) and (b) are FEM models used for loaded gear contact analyses of the reducer when the crankshaft angles are 15 and 44° respectively. Positions of the contact teeth, bushes and rollers are also numbered in Fig. 20 like Fig. 9.

Figs. 21(a) and (b) are calculated tooth contact stress distributions of the reducer when the crankshaft angles are 15 and 44° respectively. By comparing Fig. 21(a) with Fig. 14, it is found that the tooth contact stress distribution in Fig. 21(a) is different from

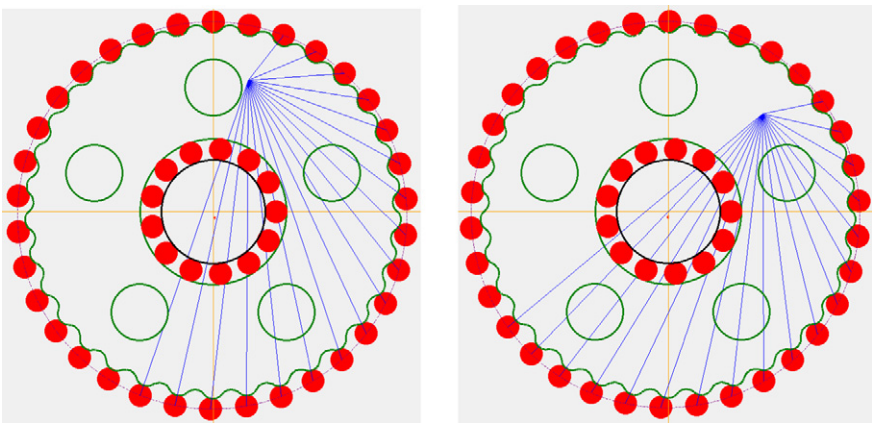

(a) Crankshaft angle=15 deg. (b) Crankshaft angle=44 deg.

Fig. 19. Tooth engagements at different angular positions of the crankshaft.

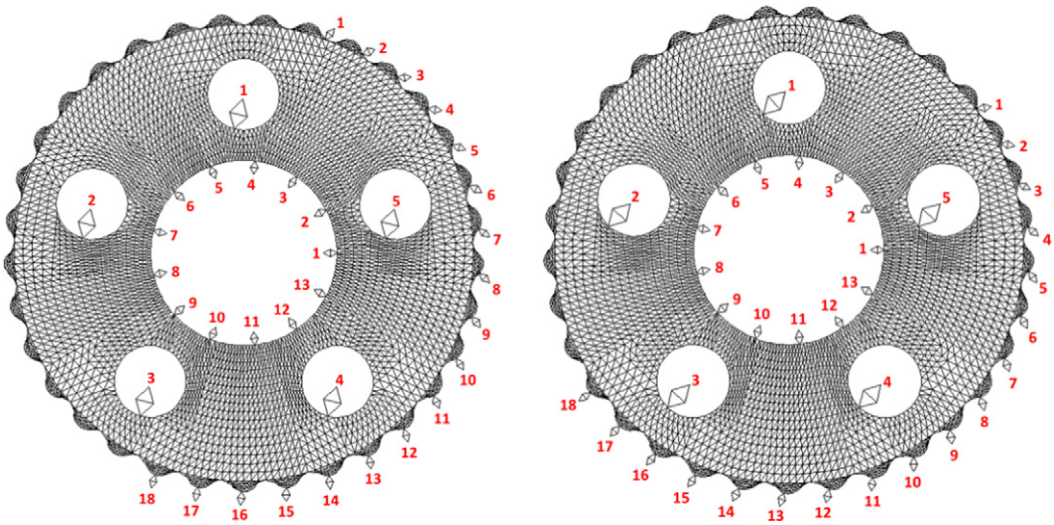

(a) Crankshaft angle=15 deg. (b) Crankshaft angle=44 deg.

Fig. 20. FEM models when the crankshaft angles are 15 and 44°.

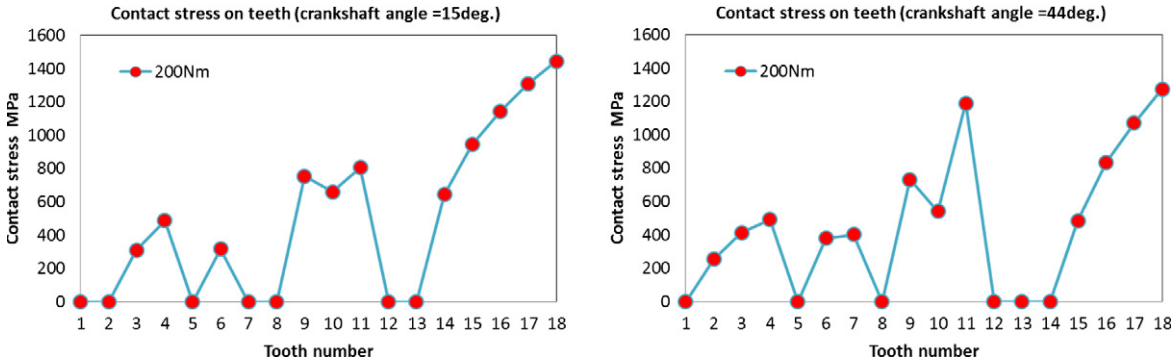

(a) Crankshaft angle=15 deg. (b) Crankshaft angle=44 deg.

Fig. 21. Tooth contact stress distribution.

the one in Fig. 14. The maximum contact stress and tooth position are also changed. Tooth contact stress distribution when the crankshaft angle is 44° is also different from the one when the crankshaft angle is 15° by comparing Fig. 21(a) with Fig. 21(b). This means that the crankshaft angle has a greater effect on tooth contact stress distribution.

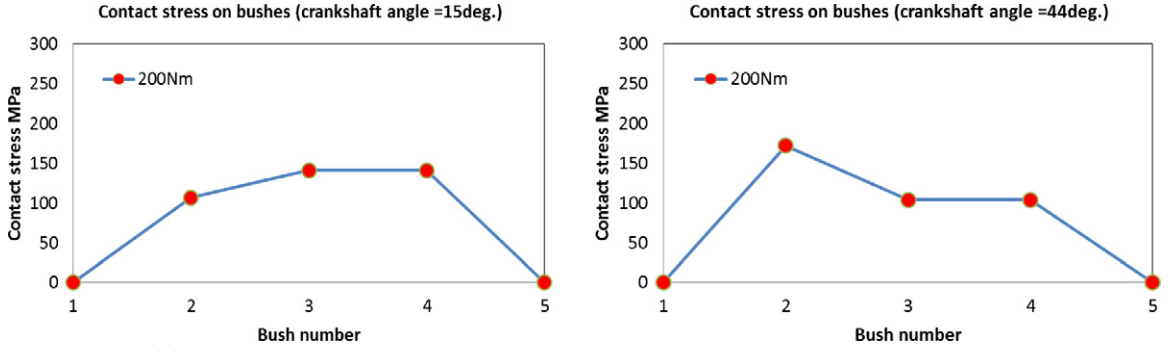

(a) Crankshaft angle=15 deg. (b) Crankshaft angle=44 deg.

Fig. 22. Bush contact stress distribution.

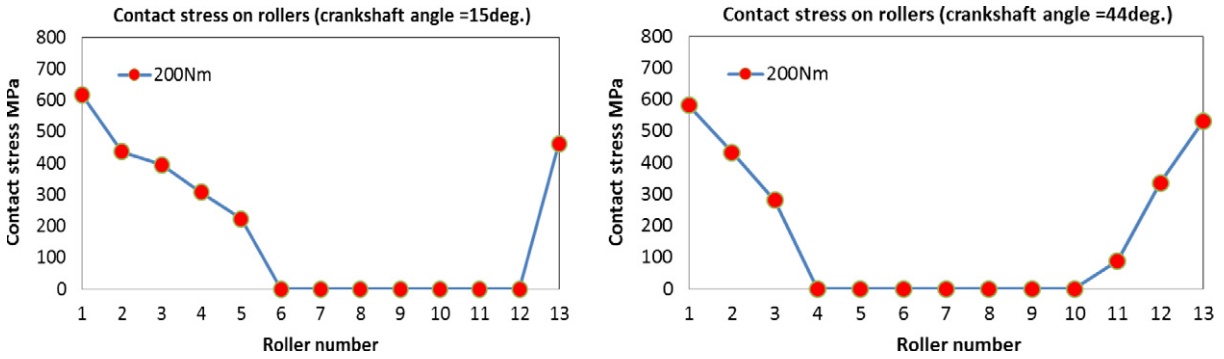

(a) Crankshaft angle=15 deg. (b) Crankshaft angle=44 deg.

Fig. 23. Roller contact stress distribution.

Fig. 22(a) and (b) is calculated bush contact stress distributions of the reducer when the crankshaft angles are 15 and 44° respectively. It is found that the crankshaft angle also has a greater effect on the bush contact stress distribution.

Fig. 23(a) and (b) is calculated roller contact stress distribution of the reducer when the crankshaft angles are 15 and 44° respectively. It is found that the crankshaft angle also has a greater effect on the roller contact stress distribution.

7. Conclusions

(1) Design software used for determining gearing parameters and structural dimensions of trochoidal gear reducers has been developed using Visual Basic language inserted AutoCAD software. With the help of the developed software, trochoidal gear reducers can be designed very simply. 2D drawings of the designed reducers can be drawn automatically on the templates of the AutoCAD software and 3D drawings of the reducers can be drawn simply using 3D commands of the AutoCAD software. This design software can not only save much time of an experienced designer, but also provide a very benefit design platform for an inexperienced designer to design and draw the reducers freely.

(2) Finite element methods used to conduct loaded gear contact analyses of the trochoidal gear reducers are presented in the paper based on a long time research. With the help of the presented methods, it becomes practical to conduct loaded gear contact analysis and strength calculations of the trochoidal gear reducers in theory. FEM programs have also been developed successfully according to the principle of the presented methods. With the help of the developed FEM programs, loads as well as contact stresses on the teeth, bushes and rollers are analyzed. Bending stress analyses of the trochoidal gear are also conducted with the finite element method.

Acknowledgments

The author was greatly indebted to Professor *Teruaki Hidaka* and Professor *Takeshi Ishida* at *Yamaguchi University* for their direct or indirect assistance in this research during 1994 and 1998.

References

[1] M. Lehman, Berechnung der Kräfte im Trochoiden-Getriebe, Antriebstechnik 18 (12) (1979) 613–616.
[2] A.K. Malhotra, M.A. Parameswaran, Analysis of a cycloid speed reducer, Mech. Mach. Theory 18 (6) (1983) 491–499.
[3] D.C.H. Yang, J.G. Blanche, Design and application guidelines for cycloid drives with machining tolerances, Mech. Mach. Theory 25 (5) (1990) 487–501.
[4] J.G. Blanche, D.C.H. Yang, Cycloid drives with machining tolerances, J. Mech. Transm. Autom. Des. 111 (1989) 337–344.
[5] T. Ishida, T. Hidaka, H. Wang, H. Yamada, M. Hashimoto, Bending stress and tooth contact stress of cycloid gear with thin rims, Trans. JSME 62 (593) (1996) 291–297 (Sec. C).
[6] Product Catalog of Nabtesco Corporation.
[7] T. Ishida, S. Li, T. Yoshida, T. Hidaka, Tooth load of thin rim cycloidal gear, Proceedings of the 7th International Power Transmission and Gearing Conference, vol.88, ASME, 1996, pp. 565–571.
[8] T. Ishida, S. Li, T. Yoshida, T. Hidaka, LE RUOTE DENTATE CICLOIDAL a corona sottile, ORGANI DI TRASMISSIONE, 1997. 48–56 ((In Italian), NOVEMBRE).
[9] T. Ishida, S. Li, T. Yoshida, T. Hidaka, Effects of tooth width, gear size, machining tolerances and loading torque on tooth load of a cycloidal gear, *JSME Mechanical Engineering Annual Meeting*, No.955-2, 1995, pp. 227–230.
[10] T. Ishida, T. Yoshida, S. Li, Relationship among face width, amount of gear error, gear dimension, applied torque and tooth load in cycloidal gears, Trans. JSME 64 (623) (1998) 2711–2717 (Sec. C).
[11] T. Ishida, Study on strength calculation problems of thin-rimmed gears, doctoral dissertation, Yamaguchi University, Japan, 1985.